

High-temperature diffusion of oxygen in synthetic diopside measured by nuclear reaction analysis

L. PACAUD, J. INGRIN AND O. JAOUl

Laboratoire d'étude des mécanismes de transfert en géologie, UMR CNRS 5563, Minéralogie, 39 allées Jules Guesde, F-31000 Toulouse, France

ABSTRACT

We have performed O self-diffusion experiments in synthetic diopside single crystals along the *b*-axis at temperatures ranging from 1473–1643 K, under controlled O partial pressure (10^{-11} – 10^{-2} atm). The ^{18}O tracer diffusion was imposed by solid/gas exchange between ^{16}O in diopside and $^{18}\text{O}_2$ -enriched argon-hydrogen- H_2O gas mixture. Diffusion profiles of ^{18}O were measured by Nuclear Reaction Analysis $^{18}\text{O}(\text{p},\alpha)^{15}\text{N}$. The diffusion coefficients are described by $D = D_0 \exp(-\frac{E}{RT})$, with $\log D_0(\text{m}^2/\text{s}) = -9.2 \pm 1.0$ and $E = 310 \pm 30 \text{ kJ/mol}$.

Our results are in agreement with Ryerson and McKeegan's (1994) data and Farver's (1989) data along a direction perpendicular to the *c* direction. Experiments performed in a wide $p\text{O}_2$ range show that D is independent of $p\text{O}_2$.

We observe no change in the diffusion regime up to 1643 K (i.e. 22 K prior to melting temperature). This result differs from the diffusion study of Ca in diopside by Dimanov and Ingrin (1995), where a strong enhancement of Ca mobility, attributed to an excess disorder in the Ca-sublattice, was observed above 1523 K. We conclude that O diffusion in diopside is not affected by this premelting phenomenon.

KEYWORDS: Nuclear Reaction Analysis, oxygen diffusion, diopside, premelting.

Introduction

THE rates of a number of geological processes, such as high-temperature creep governed by dislocation climb, oxidation and metamorphic reactions, are controlled by diffusion of the major atomic species constituting rock forming minerals. In each case, the kinetics are governed either by a simple or by a coupled diffusion process which is a function of the self-diffusion coefficients of one or several atomic species. A knowledge of the diffusion coefficients as a function of temperature and $p\text{O}_2$ is fundamental in identifying the mechanisms of elemental mobility and the nature of the point defects involved.

In diopside, it is only recently that self-diffusion data for major cations have been collected: Ca (Dimanov and Ingrin, 1995; Dimanov *et al.*, 1996); Si (Béjina and Jaoul, 1996); and Mg (Azough and Freer, 1998). On the

other hand, O self-diffusion in diopside has been studied for a decade (Connolly and Muehlenbachs, 1988; Farver, 1989; Elphick and Graham, 1990; Ryerson and McKeegan, 1994). However, these O data cover several orders of magnitude, depending on the experimental procedure and/or the nature of the diopside samples used for the experiments (see, for instance, Ryerson and McKeegan, 1994). The exact origin of these discrepancies has not been clearly identified by previous workers. The study of O diffusion in pure synthetic diopside single crystals, performed on samples previously used for the study of Ca self-diffusion in diopside (Dimanov and Ingrin, 1995), may help to identify the origin of these discrepancies and confirm the low diffusion coefficients of O.

Moreover, there are no existing data for O diffusion in diopside, at temperatures within the last 200 K before melting. The study of O diffusion in this range of temperature is of

particular interest for the understanding of the 'premelting' phenomenon that occurs above 1523 K in diopside (Fiquet *et al.*, 1992; Richet *et al.*, 1994; Dimanov and Ingrin, 1995; Richet *et al.*, 1998).

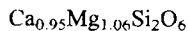
Specific heat anomalies related to 'premelting' in anorthite, pseudowollastonite, åkermanite and diopside were first indicated by calorimetric measurements showing an abnormal increase of the heat capacity, a few hundred degrees below the melting temperature (Richet and Fiquet, 1991). Transmission electron microscopy observations as well as the reversibility of the phenomenon gave Richet and Fiquet (1991) good reason to exclude partial melting as the cause of premelting. These authors suggested that premelting is related to an unquenchable structural change.

In pure synthetic diopside, premelting starts at ~1523 K, the same temperature as the increase of Ca mobility observed by Dimanov and Ingrin (1995). Those authors concluded that Ca diffusion in diopside is affected by premelting. They suggested that a thermal excess of point defects, Ca-Frenkel defects, may explain the phenomenon. Such defects should only affect the Ca-sublattice. To test this hypothesis, we undertook an experimental study on O diffusion, at temperatures greater and less than 1523 K, to check whether the anionic sublattice could be influenced by premelting phenomenon.

Experimental procedures

Sample preparation

The samples used in this study are identical to those prepared by Dimanov and Ingrin (1995) for their Ca diffusion study. Samples were prepared from a synthetic diopside single crystal provided by S.R. Hart and V. Sautter from Sneeinger's collection (Sneeinger *et al.*, 1984). The chemical composition of the crystal was determined using a Cameca SX50 electron microprobe at the Université Paul Sabatier (Toulouse, France). The analytical conditions were 15 kV and 20 nA, using natural and synthetic standards:



The concentration of Fe was below the detection limit of the microprobe and was estimated at <0.3 at.% Fe/(Fe+Mg).

Specimens were oriented using the X-ray Laue technique within a precision of 5°, with their larger faces perpendicular to [010]. The very short

distances of diffusion required high-quality surfaces. Oblong 6 mm² slices, 1 mm thick, were polished with alumina powder of decreasing grain size down to 0.3 µm. After polishing, the slices were etched in hydrofluoric acid, diluted to 50%, in order to remove the cold-worked zone produced at the surface by mechanical polishing. For this study, we used ten slices labelled in alphabetic order a to j. Most samples were used several times for different runs. After analysis, they were systematically re-polished and etched.

For Nuclear Reaction Analysis (NRA) and Rutherford Backscattering Spectrometry Analysis (RBS), the annealed samples were glued onto copper supports and a thin film of amorphous carbon was evaporated on the surface to avoid charging during ion beam irradiation in the accelerator.

Oxygen diffusion experiments

Table 1 gives the experimental conditions and results. The annealing runs were performed in the 1473–1643 K range in a horizontal alumina tubing heated externally by a lanthanum chromite resistor (Pyrox, VG 30 furnace). In order to prevent contamination by alumina or other elements present in the tubing, the samples were placed in a platinum crucible in the central part of the furnace. The temperature was monitored by a Pt/Pt-10%RR thermocouple located a few mm from the samples. The temperature gradient in the central part of the furnace (5 cm) was <~0.5 K/cm, and the temperature uncertainty was estimated at <± 5 K. The heating and cooling duration (~1 h in total) were short compared to annealing duration so that the diffusion profiles were not significantly affected.

Diffusion of ¹⁸O tracer was performed by a direct gas-solid exchange between an ¹⁸O-enriched atmosphere and the polished sample surface. The isotopic source for tracer diffusion is a mixture of argon and H₂ flowing through ¹⁸O-enriched water (10 to 50%). The resulting H₂O vapour pressure ($p_{\text{H}_2\text{O}} = 0.026 \text{ atm}$ at 295 K; Weast and Astle, 1979) imposed the p_{O_2} in the furnace which was controlled by a zirconia probe (SIRO₂ sensor). The most oxidizing regime was obtained with pure Ar flowing through water, leading to a p_{O_2} of $8 \times 10^{-2} - 1.5 \times 10^{-3} \text{ atm}$, depending on temperature, and the most reducing experiments (p_{O_2} between 10^{-10} and 10^{-12} atm) were obtained with Ar/10% H₂ flowing through water.

OXYGEN DIFFUSION IN DIOPSIDE

TABLE 1. The samples are labelled a, b ... j. The number which follows corresponds to the number of annealings of the same specimen

Sample	Temperature (K)	Annealing duration (h)	$p\text{O}_2$ (atm)	$2\sqrt{Dt}$ (nm)	D (m^2/s)	C_0
h1 *	1473	79	2.1×10^{-2}	80	5.6×10^{-21}	0.1
i4	1473	240	8.1×10^{-2}	150	6.5×10^{-21}	0.05
f3	1473	456	7.7×10^{-2}	230	8×10^{-21}	0.05
b1 *	1523	24	9.8×10^{-3}	90	2.3×10^{-20}	0.1
a1	1523	48	1.2×10^{-2}	130	2.4×10^{-20}	0.1
a2	1523	96	5.6×10^{-3}	110	8.7×10^{-21}	0.2
c1 **	1523	360	2.2×10^{-3}	220	9.3×10^{-21}	0.2
j2	1523	720	2.2×10^{-3}	400	1.5×10^{-20}	0.08
e5	1523	310	9.8×10^{-11}	270	1.6×10^{-20}	0.085
e1	1573	24	5.4×10^{-3}	115	3.8×10^{-20}	0.25
i1	1573	48	1.3×10^{-3}	145	3×10^{-20}	0.2
h2	1573	96	2.9×10^{-2}	230	3.8×10^{-20}	0.08
e2 **	1573	192	2.9×10^{-3}	225	1.8×10^{-20}	0.15
e3 **	1573	384	1.8×10^{-3}	300	1.6×10^{-20}	0.15
f4	1573	96	1×10^{-10}	180	2.3×10^{-20}	0.07
j3 **	1573	200	4.4×10^{-11}	330	3.8×10^{-20}	0.06
f1	1623	24	1.8×10^{-2}	175	8.9×10^{-20}	0.15
i2 **	1623	48	2.9×10^{-2}	220	7×10^{-20}	0.1
h3	1623	96	2.2×10^{-3}	260	4.9×10^{-20}	0.15
f2 **	1623	189	1.7×10^{-3}	410	6.2×10^{-20}	0.08
i3	1643	41	2.6×10^{-3}	220	8.2×10^{-20}	0.1
d2 **	1643	72	1.5×10^{-3}	350	1.2×10^{-19}	0.1

* The profile width is too close to the resolution (~ 60 nm), and the uncertainty of such data is much greater than for other profiles. We did not take these data into account for the calculation of the activation energy.

** Etch pits observed at the surface of the sample.

The initial H_2^{16}O present in the gas (Ar or Ar/10% H_2) from the commercial container was removed by freezing at 263 K at the entry of the alumina tubing prior to mixing with H_2^{18}O . The ^{18}O -enriched water contained in the gas after its travel through the furnace was also freeze-dried at 263 K for reuse.

After each run, the sample surface was observed carefully using an optical microscope. Except for small etch-pits in a few experiments with $T \geq 1573$ K, the surface of the samples remained almost unaltered (Table 1).

Analytical procedures

Oxygen profile measurement

Each sample was initially analysed by Rutherford Backscattering Spectrometry (RBS). The sample surface was irradiated using a beam of 2 MeV

α -particles generated by a Van de Graaff accelerator (GDR 86, groupe de physique du solide, Université de Paris-Jussieu). The α -particles collide on nuclei of the target (Ca, Mg, Si, O) and rebound in different directions. Part of these α -particles are collected by a silicon detector at angle $\theta = 15^\circ$ to the incident beam. A multichannel analyzer sorts α -particles as a function of their energy. The RBS can distinguish the rebounds of α -particles on the different nuclei and collisions at different depth. Figure 1 shows a typical α -RBS spectrum in diopside exposed to $^{18}\text{O}_2$.

Systematic RBS analyses were performed on samples prior to NRA analyses in order to check the surface chemical composition and if necessary change the orientation of the target under the beam to avoid channelling of incident particles along preferential crystallographic orientations.

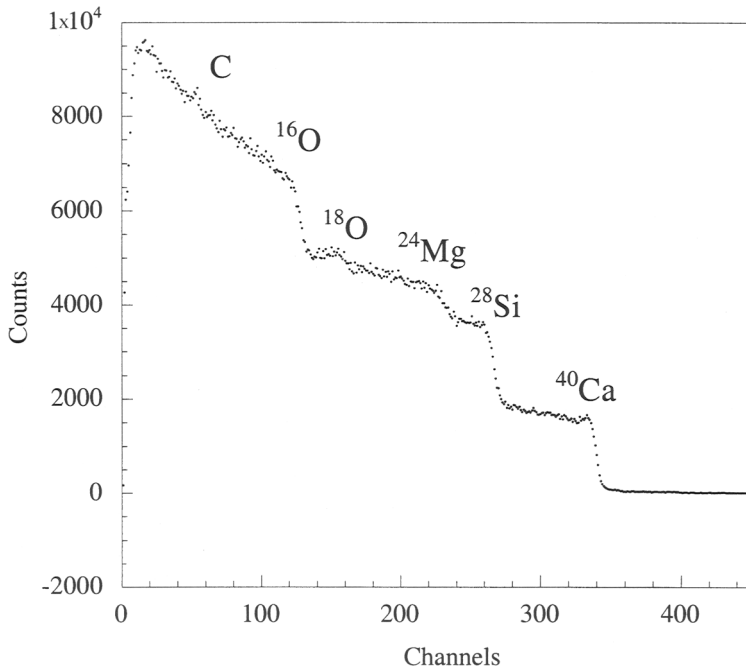
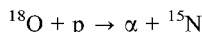


FIG. 1. RBS spectrum of the sample (a1) showing the number of α -counts as a function of their energy. Each plateau corresponds to a different isotope. The height of the plateau is proportional to the abundance of the element. The position of the vertical edges corresponds to the energy of retrodiffusion of α -particles at the surface for each element. A small diffusion profile of ¹⁸O is evidenced by the small bump in front of the ¹⁶O edge. A sharp peak around channel 55 corresponds to the evaporated film of carbon on the surface of the sample.

This phenomenon could lead to an overestimation of the value of diffusion coefficients (L'hoir *et al.*, 1981; Jaoul *et al.*, 1983). Channelling is detected when edges (shown in Fig. 1 for Ca and Si elements for instance) on RBS spectra lose their angular shape and become rounded.

The RBS spectrum shows the presence of ¹⁸O at and below the surface by the existence of a diffuse step between ¹⁶O and ²⁴Mg plateaux. However, the difference in mass between ¹⁸O and ¹⁶O is too small to allow a good deconvolution of the ¹⁸O plateau which also has a weak signal to noise ratio.

The concentration profiles of ¹⁸O were obtained by specific ¹⁸O Nuclear Reaction Analysis which allows measurement a few μm beneath the sample surface, with good resolution. A 740 keV incident proton beam (1 or 2 mm diameter) reacts with the ¹⁸O nuclei contained in the sample according to the equation:



Technical details about this now classical method can be found in Reddy *et al.* (1980), L'hoir *et al.* (1981) and Jaoul *et al.* (1983).

A germanium detector measures the energy of the emitted α -particles at an angle of $\theta = -30^\circ$ relative to the incident proton beam (Fig. 2).

The energy E_α of the detected α -particles is directly related to the depth of the nuclear reaction beneath the surface and the number of collected α -particles originating from a given depth is proportional to the ¹⁸O concentration at this depth.

E_α is a function:

(1) of proton energy $E_p(x)$ arriving at the depth x (Fig. 2). $E_p(x)$ is equal to the incident energy $E_p(0) = 740$ keV, minus the energy lost during travelling within the sample from 0 to x :

$$E_p(x) = E_p(0) - \int_0^x S_p dx$$

OXYGEN DIFFUSION IN DIOPSIDE

The stopping power S_p depends on the nature of the material and on the proton energy and thus on depth. From tables by Ziegler and Biersack (1985), we have:

$$S_p (\text{eV}/\text{\AA}) = 16.7 - 1.8 \times 10^{-8} E_p(x) (\text{eV}) + 7.4 \times 10^{-15} E_p^2(x) (\text{eV})$$

(2) the energy $E_\alpha(x)$ of the emitted α -particle from a ^{18}O nucleus, at depth x , is a function of $E_p(x)$ following the kinematic equation (Cawley, 1984):

$$E_\alpha(x) (\text{keV}) = 3002.724 + 0.482 E_p(x) (\text{keV})$$

(3) the energy loss of the α -particles along a length $x/\cos\theta$ when travelling within the sample toward the detector (Fig. 2). From the tables by Ziegler and Biersack (1985), the stopping power S_α of the α -particles in diopside is:

$$S_\alpha (\text{eV}/\text{\AA}) = 60.8 - 1.4 \times 10^{-8} E_\alpha(x) (\text{eV}) + 1.3 \times 10^{-15} E_\alpha^2(x) (\text{eV})$$

The detected energy is:

$$E_\alpha = E_\alpha(x) - \int_0^{x/\cos\theta} S_\alpha dx$$

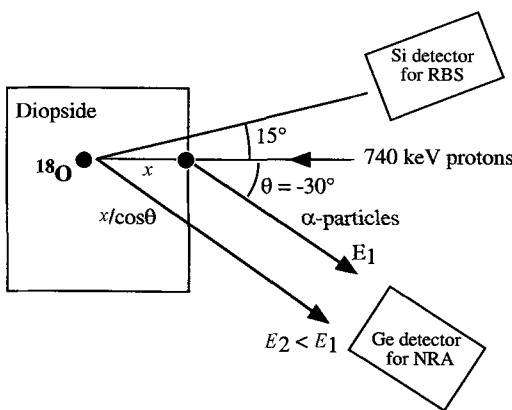


FIG. 2. Schematic diagram of RBS and NRA experiments: A 740 keV incident proton beam penetrating the diopside target. The RBS Si-detector of protons is at angle of $\theta = 15^\circ$ and the NRA detector of α -particles is at an angle of $\theta = -30^\circ$. Knowledge of the energy loss, along the inward path (x) of protons and along the outward path ($x/\cos\theta$) of α -particles, allows us to calculate the depth of the reaction (x) from the energy of detected α -particles.

For $x < 1000$ nm, E_α and x can be described by a linear relation, according to:

$$\frac{\Delta E_\alpha}{\Delta x} = k \text{ with } k = 0.37 \text{ keV/nm.}$$

The number of detected α -particles at a given energy is function of several parameters: (1) the ^{18}O concentration at a given depth. (2) The number of incident protons which is related to the beam intensity. It corresponds to an exposure duration of the sample to the beam multiplied by the intensity of the beam current (between 30 and 270 nA). The total charge ranged from 10 to 90 μC in all our experiments. (3) The detection solid angle $\delta\Omega$ of the detector. (4) The differential cross section of the reaction $d\sigma/d\Omega$ which is a function of proton energy. The value 740 keV corresponds to a high value of $d\sigma/d\Omega$ (≈ 15 millibarn/steradian), leading to a good efficiency of the nuclear reaction and therefore to good counting statistics. Moreover, in this range of energy, the differential cross section does not vary much with proton energy (Jaoul *et al.*, 1991). At a depth of 400 nm, the protons have lost 30 keV: this is equivalent to a variation of the cross section of 2 mb/sr. We have taken this effect into account, which is however, too small to affect the simulation of the experimental profiles.

Thus, a NRA spectrum (number of α counts vs their energy, Fig. 3) represents a picture of the ^{18}O concentration as a function of sample depth.

The resolution in energy of the analyses was measured by performing a NRA analysis on a tantalum oxide $\text{Ta}_2^{18}\text{O}_5$ thin layer, the thickness of which (15 nm) was negligible compared to the resolution. This gives the instrumental resolution function, a pseudo gaussian function, which is simply due to the detector resolution itself and the straggling effect. Straggling is the energy dispersion as a function of depth, due to interactions of particles with the material: the deeper the reaction occurs, the higher the uncertainty on the energy values. We used a straggling value of $0.19 \text{ keV nm}^{-1/2}$.

The resolution of the detector, extracted from the $\text{Ta}_2^{18}\text{O}_5$ spectrum is equal to 23 keV. It corresponds to a resolution in depth of 60 nm.

The correspondence between channel and energy (Fig. 3) is determined from the known energy (3.359 MeV) of the α -particles produced at the surface (middle of the front edge of the spectrum) and the calibration energy/channel of the detection chain.

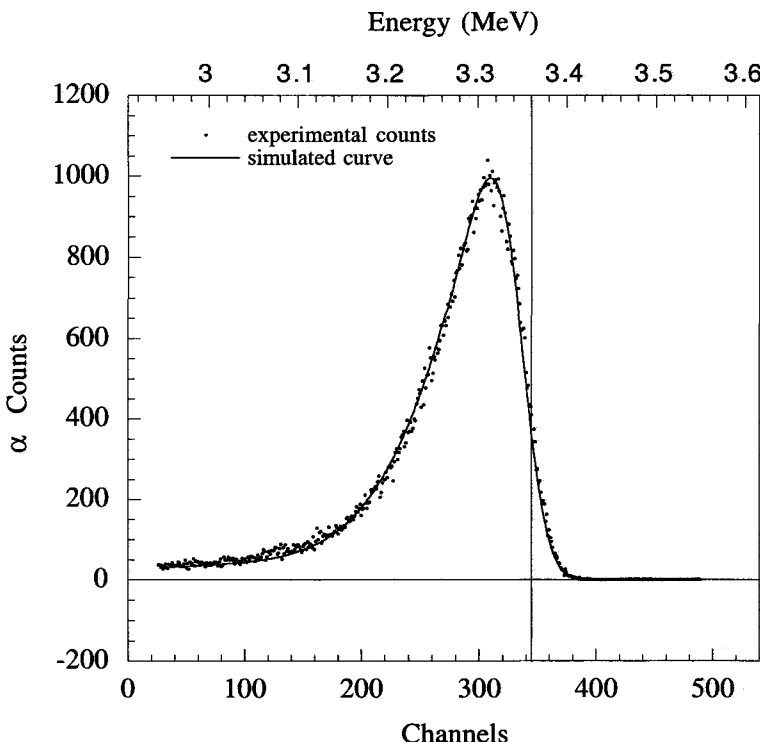


FIG. 3. Typical NRA spectrum: number of detected α -particles as a function of their energy (1 channel = 1.31 keV = 3.5 nm). The experimental data of sample f2 are shown by dots. The solid line is the result of the fit. The sample was annealed at 1623 K for 189 h with $pO_2 = 1.7 \times 10^{-3}$ atm. The diffusion coefficient deduced from this fit is $6.2 \times 10^{-20} \text{ m}^2/\text{s}$. The surface of the sample is represented by the vertical line.

Determination of the diffusion coefficients

To extract diffusion coefficients from the NRA profiles, we performed numerical simulations by convoluting the solution of the diffusion law (1) with the instrumental function.

The boundary conditions of our experiments are such that the ^{18}O concentration as a function of depth and annealing duration (t) is:

$$C(x, t) = C_\infty + (C_0 - C_\infty) \operatorname{erfc} \left(\frac{x}{2\sqrt{Dt}} \right) \quad (1)$$

where C_∞ is the natural isotopic abundance ($C_\infty = 0.2\%$), C_0 is the isotopic surface concentration fixed by the gas mixture, and erfc is the complementary error function. D is the diffusion coefficient and $2\sqrt{Dt}$ is the characteristic diffusion length and can reach a few hundreds of nm.

In fact, C_0 has different values in each of our experiments because the enrichment of H_2^{18}O was different as was the imposed pO_2 . However,

this has no effect on the characteristic diffusion length.

The solution of Fick's law (1) is convoluted with the Gaussian instrumental function $G(x)$:

$$G(x) = \frac{1}{\sqrt{2\pi}\sigma} \exp \left(-\frac{x^2}{2\sigma^2} \right)$$

in which σ (nm) = $\frac{1}{k}\Sigma$ (keV), where Σ is related to the detector resolution (R) and straggling effect (T):

$$\Sigma(x) = \sqrt{(R^2 + T^2)x}$$

with $R = 23$ keV and $T = 0.19$ keV nm $^{-1/2}$.

Data are fitted using the result of the convolution, adjusting two parameters: $2\sqrt{Dt}$ and C_0 .

Results

The diffusion data are listed in Table 1. For each run, we give temperature, annealing duration,

OXYGEN DIFFUSION IN DIOPSIDE

pO_2 , $2\sqrt{Dt}$, D the deduced diffusion coefficients and C_0 the isotopic surface concentration. The measured values of D range from 5.6×10^{-21} to $1.2 \times 10^{-19} \text{ m}^2/\text{s}$ for temperatures between 1473 K and 1643 K. Oxygen diffusion in diopside is very slow: in order to obtain $2\sqrt{Dt} = 200 \text{ nm}$ at 1473 K, the annealing duration is 20 days.

Figure 4 shows some examples of profiles obtained at $T = 1573 \text{ K}$ for different durations. We verify with such data that D is independent of the annealing duration (t) at any given temperature (Fig. 5). It confirms that the characteristic diffusion length is effectively proportional to \sqrt{t} (except for short annealing durations where $2\sqrt{Dt}$ is close to the detector resolution ($\sim 60 \text{ nm}$, Table 1)).

The quality of the fit of the data is such that we are able to discriminate between two values of D with a difference of $< 10\%$, i.e. 0.05 log unit on D . We conclude that the fit itself contributes little to the error on D . The main uncertainties arise from the reproducibility of experimental measurements, mainly affected by the different quality of the surfaces of the samples, accelerator setting, etc. In general with NRA analyses, an uncertainty

of $< \pm 0.5$ in $\log D$ can be assumed (Gérard and Jaoul, 1989; Jaoul *et al.*, 1991; Dimanov *et al.*, 1996).

In order to obtain some information on a possible diffusion mechanism, we have investigated the dependence of D on pO_2 . We have performed reducing anneals at two different temperatures, 1523 K and 1573 K. We observed no difference in D within experimental uncertainties for these two temperatures (Figs 5, 6), despite the large range of pO_2 covered by these experiments (more than eight orders of magnitude). We thus conclude that the mechanism of O diffusion in synthetic diopside in the b direction is independent of pO_2 , at least in the range of temperature and pO_2 investigated here.

One usually writes:

$$D = D_0 \exp\left(-\frac{E}{RT}\right)$$

with D_0 , the pre-exponential factor, R the gas constant, E the activation energy which is related to the energy of formation and migration of the defect involved in the diffusion process. An

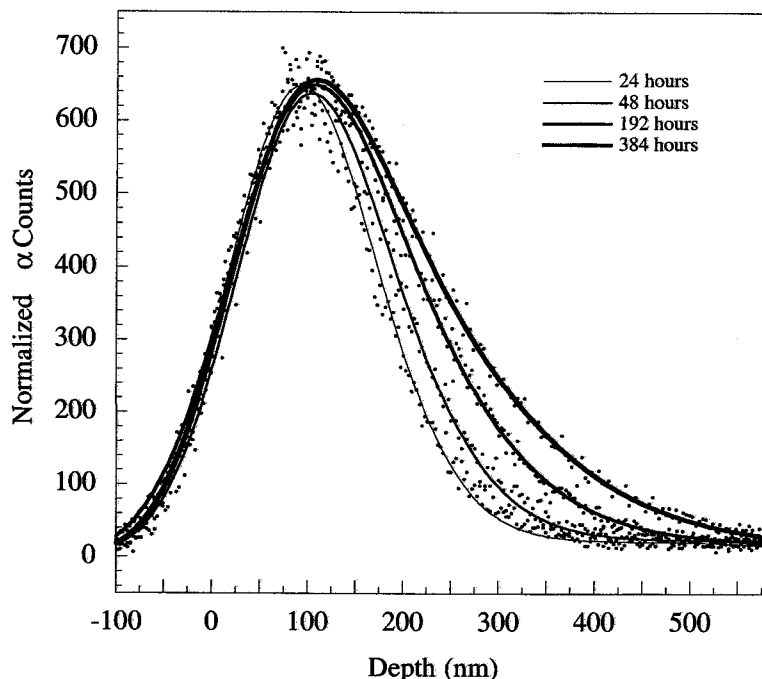


FIG. 4. Experimental profiles and their fit for different annealing durations at $T = 1573 \text{ K}$.

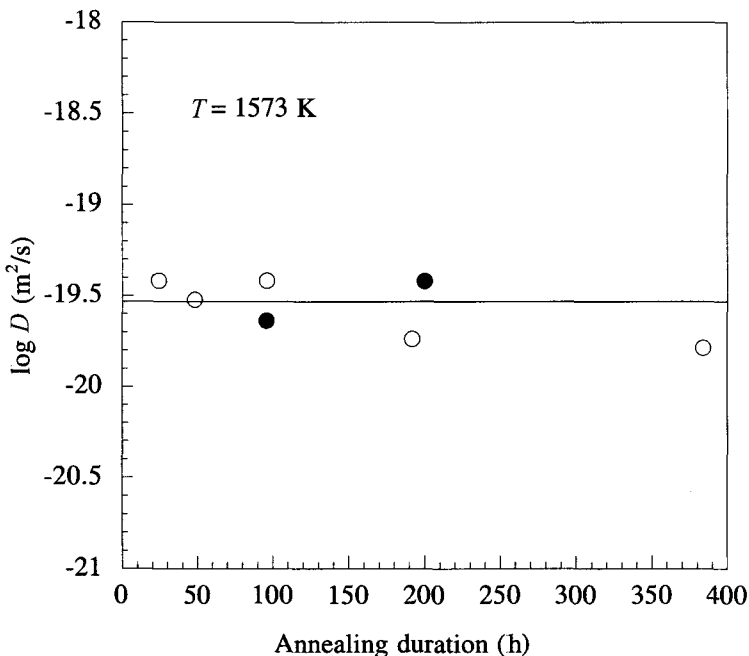


FIG. 5. $\log D$ (m^2/s) as a function of annealing duration at $T = 1573$ K for oxidizing (empty circles, $p\text{O}_2 \approx 10^{-2}$ atm) and reducing conditions (filled circles, $p\text{O}_2 \approx 10^{-10}-10^{-11}$ atm.; see Table 1). The independence of D on time shows that equation (1) is adapted to our experimental conditions. Uncertainty with $\log D$ data is taken as ± 0.5 .

Arrhenius plot of $\log D$ vs $10^4/T$ with a least squares fit (York, 1966) of the data (all data except short profiles data) yields:

$$D(\text{m}^2/\text{s}) = 5.8^{[+51.2]}_{[-5.2]} \times 10^{-10} \exp\left(-\frac{310 \pm 30 \text{ kJ mol}^{-1}}{RT}\right)$$

i.e. $\log D_0$ (m^2/s) = -9.2 ± 1.0

The standard deviations of the pre-exponential factor and the activation energy were calculated with York's method assuming an error of ± 0.5 in $\log D$ and ± 5 K in T .

The data collected for ^{18}O at high temperature show that there is no drastic change in the slope of the Arrhenius plot at temperatures less than and greater than 1523 K, as has been observed for Ca diffusion (Dimanov and Ingrin, 1995) (Fig. 8).

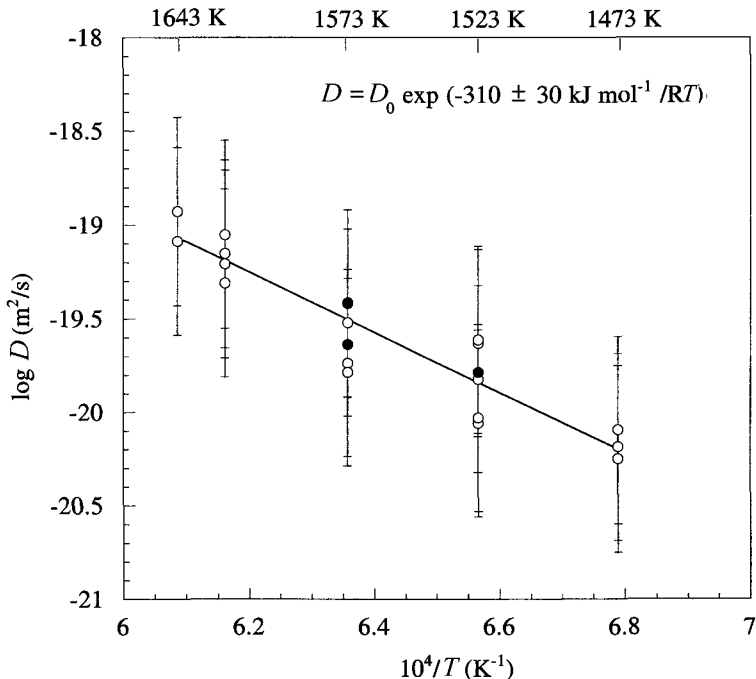
Discussion

Comparison with other O diffusion data

Comparison of our data with previous studies of O diffusion in diopside is shown in Fig. 7 and Table 2. We think that the dispersion of the

different data is mainly due to differences in crystal composition, experimental conditions and analytical procedures.

The O diffusion data of Connolly and Muehlenbachs (1988) are the only data collected on synthetic samples with a composition identical to ours. However, these authors used polycrystalline samples (grain size 25 μm). The diffusion coefficients were deduced from the measurement of the isotopic composition of the powder assuming an isotropic spherical model for diffusion. We know that the major problem encountered by the use of crushed material to determine bulk diffusion coefficients is the difficulty in determining precisely the grain size and shape of the particles (Ando and Oishi, 1983; Ryerson and McKeegan, 1994). The surface: volume ratios of crushed particles are generally underestimated, leading systematically to diffusion coefficients one or two orders of magnitude greater than coefficients deduced from bulk diffusion experiments (Ando and Oishi, 1983). This is the order of magnitude of the discrepancy that we observe between our data and the data



G. 6. Arrhenius plot $\log D$ (m^2/s) vs $10^4/T$ (K^{-1}). Filled circles are for reducing conditions and open circles for oxidizing conditions. The activation energy, given by the slope, is $310 \pm 30 \text{ kJ/mol}$.

from Connolly and Muehlenbachs (1988) (1.5 to 2 orders; Fig. 7). These results are not considered further.

Table 2 shows a compilation of all the available data with recalculated values of E and D_0 from the original data points by York's (1966) method which takes into account the uncertainty in both T and D . This permits better comparison of different O diffusion data. The use of a common fitting method reduces substantially the discrepancy among the deduced activation energies of O diffusion (range 240 to 400 kJ/mol; Table 2). Our 310 kJ/mol corresponds roughly to the average value of the all reported activation energies.

The diffusion data collected by Ryerson and McKeegan (1994) are in relatively good agreement with our results taking into account the uncertainty in the diffusion coefficients (± 0.5 log unit on D ; Fig. 7). Ryerson and McKeegan's (1994) diffusion data were collected along c and the Fe content of the samples was 2.1, 4.4 and 7.8 at.% Fe/(Fe+Mg). The samples were annealed under dry conditions. The slightly higher values

of the diffusion coefficients might be explained by the difference in Fe content of their samples compared to our synthetic samples. Those authors noticed almost no difference in diffusion in the range of Fe content that they explored; however our samples are considerably poorer in Fe (8–20 times less Fe). Another explanation for the slight difference from our data may arise from a possible anisotropy of diffusion between the b and c crystallographic directions. No attempt at measurement of diffusion along b was performed by Ryerson and McKeegan (1994) in order to confirm such an assumption.

In his experiments performed on a gem quality natural single crystal from Tyrol (Austria), with unknown but very low Fe content, Farver (1989) observed a strong effect of anisotropy of diffusion between the c direction and an unknown direction, perpendicular to c . His data along the direction perpendicular to c are very close to those in the present work, within 0.5 of an order of magnitude. However, the activation energy is somewhat lower: $227 \pm 48 \text{ kJ/mol}$ (Fig. 7, Table 2). The small discrepancy with our data, collected along

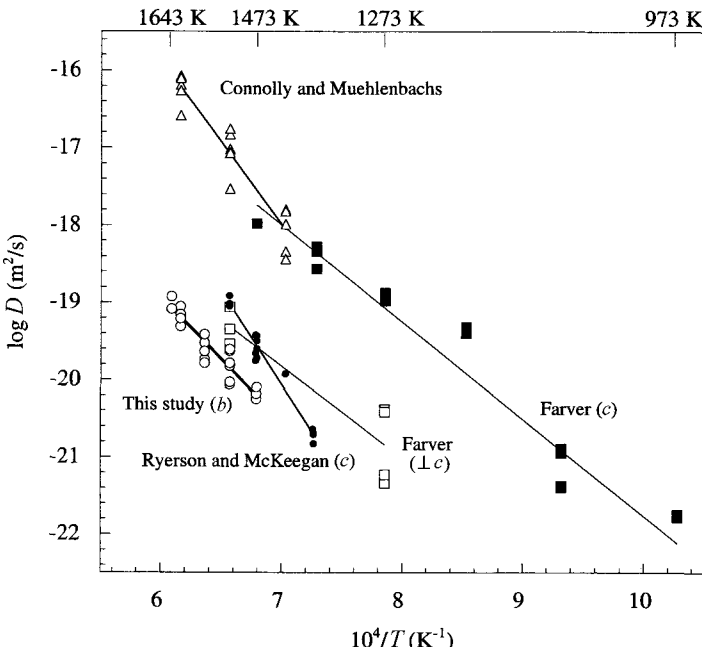


FIG. 7. Comparison with published data on oxygen in diopside. Farver (1989) $\perp c$ (open squares), $\parallel c$ (filled squares); Ryerson and McKeegan (1994) $\parallel c$ (filled circles); Connolly and Muehlenbachs (1988) (open triangles); present study (open circles).

b, may simply result from a small difference in composition compared to our synthetic crystal or a small anisotropic effect. Farver's experiments were performed under hydrous conditions and a confining pressure of 100 MPa. It has been widely suggested that O diffusion in minerals may be enhanced by the presence of water (Giletti and Yund, 1984; Giletti, 1985; Elphick and Graham, 1988; Farver and Yund, 1990; Farver and Yund, 1991). However, if such an effect (higher diffusivity) exists for diopside, our data compared to Farver's data ($\perp c$) suggest that at least for this direction, the effect is quite small.

The anisotropic effect measured by Farver (1989) is very high (almost two orders of magnitude) (Fig. 7). His data along c disagree with the data obtained by Ryerson and McKeegan (1994) for the same crystallographic direction. The discrepancy between these two sets of data collected using very similar methods of sample preparation and analysis (see Ryerson and McKeegan, 1994) may have the following origins: (1) a very strong water effect on diffusion along c . However, reported data from Elphick and Graham (1990) collected at 1 kbar H_2O along the

same direction give diffusion coefficients almost one order of magnitude lower. (2) A shortcut of diffusion along the c direction in Farver's samples. Some of the gem quality single crystals of diopside coming from Austria are known to contain small amphibole lamellae which developed along (010) planes (Ingrin *et al.*, 1989; even for some colourless gem quality samples from Tyrol: Ingrin, unpubl. data). These amphibole exsolution can be identified easily by IR spectroscopy. Faster diffusion along these amphibole lamellae could eventually explain Farver's data along c .

The independence of the diffusion coefficients from pO_2 has already been suggested by Ryerson and McKeegan (1994). These authors performed experiments at 1378 K at $pO_2 = 10^{-10} - 10^{-13}$ atm. We observed the same behaviour in our samples on a much larger range of pO_2 ($10^{-10} - 10^{-2}$ atm.).

Premelting phenomenon

Our results show only one diffusional regime between 1473 K and 1643 K with a unique

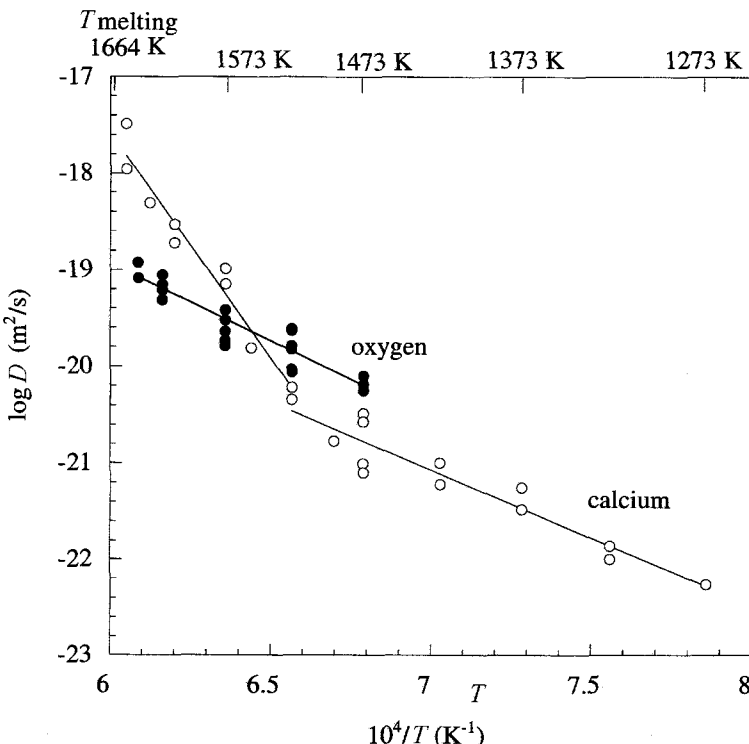


FIG. 8. Comparison of O (filled circles) and Ca (open circles; Dimanov and Ingrin, 1995) diffusion coefficients in the same synthetic diopside samples.

activation energy $E = 310 \pm 30 \text{ kJ/mol}$, as opposed to the results obtained for Ca diffusion in the same synthetic diopside (Dimanov and Ingrin, 1995) (Fig. 8). These authors found two different regimes of diffusion with an enhancement of Ca mobility above 1523 K at the same temperature as the onset of premelting (calorimetric data; Richet *et al.*, 1994; an enhancement of specific heat above 1523 K). The excess enthalpy recorded by calorimetric data could be interpreted as an anomalous excess of point defects at $T \geq 1523 \text{ K}$. Dimanov and Ingrin (1995) have proposed that the concentration of point defects involved in Ca mobility at $T < 1523 \text{ K}$ is surpassed by another population of defects at $T \geq 1523 \text{ K}$ which of course has a higher formation energy. Ca-Frenkel pairs (association of an interstitial and a vacancy) are the proposed candidates.

The absence of enhancement in O diffusion in the temperature range of premelting suggests that premelting does not affect the O sublattice. This result confirms that premelting only affects the cationic sublattice.

Richet *et al.* (1998) also interpret their calorimetric anomalies related to premelting in terms of increasing defect concentration near the melting point, but alternatively they propose an extensive dynamic exchange of Ca and Mg over available crystallographic sites in the structure. The present results on O diffusion are compatible with both interpretations and cannot discriminate between the two models.

Point defects involved in O diffusion

It is generally rather difficult to interpret O diffusion in terms of point defect chemistry and to identify the nature of the defects involved in the diffusion process, even for silicates with a simple chemical composition compared to diopside (i.e. forsterite, Jaoul *et al.*, 1980; Reddy *et al.*, 1980; Jaoul *et al.*, 1983; olivine, Gérard and Jaoul, 1989). The $p\text{O}_2$ variation of point-defect concentrations deduced from a chosen model is highly dependent on the hypothesis assumed for the charge-neutrality conditions ensuring the bulk

TABLE 2. Summary of O diffusion data in diopside. We give the temperature range, $\log D_0$ and E published by the authors (a). We have recalculated $\log D_0$ and E from their original data using the fitting method of York (1966) (b)

References	Temperature range (K)	$\log D_0$ (m^2/s) (a) original	E (kJ/mol) (a) original	$\log D_0$ (m^2/s) (b) re-calculated	E (kJ/mol) (b) re-calculated
Connolly and Muehlenbachs (1988)	1423–1623	−3.2	405 ± 24	-3.2 ± 1.2	404 ± 34
Farver (1989) $\parallel c$	973–1473	−9.8	226 ± 21	-9.2 ± 0.7	240 ± 15
Farver (1989) $\perp c$	1273–1523	−11.5	226	-11.5 ± 1.8	227 ± 48
Ryerson and McKeegan (1994) $\parallel c$	1377–1524	-3.4 ± 0.9	457 ± 26	-5.4 ± 1.2	398 ± 33
This study $\parallel b$	1473–1643			-9.2 ± 1.0	310 ± 30

electro-neutrality of the crystal (Stocker and Smyth, 1978; Stocker, 1978, for forsterite).

At least two different point defect models have so far been developed for diopside: one by Huebner and Voigt (1988) to interpret the results of electronic conductivity measurements and another by Jaoul and Raterron (1994) in order to explain SiO_2 precipitation in diopside. In these models the authors assume that $M1$ and $M2$ sites are similar (structural formula can in a first approximation, be described by $Me\text{SiO}_3$, $Me = \text{Ca or Mg}$). Both models apply to natural diopside with a substantial amount of Fe. In this case, the expected majority defects are assumed to be Me -vacancies (V''_{Me}) and Fe^{3+} in octahedral sites ($\text{Fe}^{\bullet\bullet}_{Me}$). In our synthetic Fe-free diopside, in intrinsic conditions at high temperature, such a hypothesis is no longer valid and majority defects could be Frenkel pairs ($V''_{Me}, Me^{\bullet\bullet}$). These later defects are also those proposed by Dimanov and Ingrin (1995).

Unfortunately, in the present work, as for forsterite, the independent observation of the O diffusion coefficients with $p\text{O}_2$ prevents any identification of the diffusion mechanism: interstitial (O_1'') or vacancy ($V_O^{\bullet\bullet}$). Both defects, V_O'' and O_1'' have the same theoretical dependence on $p\text{O}_2$ (i.e. $p\text{O}_2^0$; Stocker, 1978).

Conclusion

The nuclear reaction analysis technique displays several advantages in this study: specificity of the reaction to the ^{18}O isotope, good resolution in depth profiles, and non-destructive analysis of the

diopside samples. It allowed measurement of short profiles ($2\sqrt{Dt} = 80$ –410 nm) and thus, the determination of very low diffusion coefficients. Oxygen self-diffusion coefficients between 1473 K and 1643 K ranged from 5.6×10^{-21} to $1.2 \times 10^{-19} \text{ m}^2/\text{s}$. The results show only one diffusion regime with an activation energy of $310 \pm 30 \text{ kJ mol}^{-1}$ and a pre-exponential factor $D_0 = 5.8 \times 10^{-10} \text{ m}^2/\text{s}$. The experiments indicate that premelting effects which occur in diopside, do not affect the O sublattice. Two types of defects have been proposed to explain the origin of premelting: Ca-Frenkel (Dimanov and Ingrin, 1995) and Mg-Ca disorder (Richet *et al.*, 1998). Our results confirm that in either case, the defects involved in this phenomenon do not affect the anionic sites of diopside. Finally, we have shown that O partial pressure has no influence on O diffusion along b in diopside.

Acknowledgements

This work was supported by the CNRS-INSU (INSU contribution #137, program 97 IT 62; GDR 86 directed by G. Amsel). We are grateful to S.C. Elphick for his valuable comments. We would like to thank E. d'Artemare for his helpful presence during the NRA and RBS analyses, and Philippe de Parseval for the microprobe analyses.

References

- Ando, K. and Oishi, Y. (1983) Effect of ratio of surface

- area to volume on oxygen self-diffusion coefficients determined for crushed $\text{MgO}-\text{Al}_2\text{O}_3$ spinels. *J. Amer. Ceram. Soc.*, **66**, C131–2.
- Azough, F. and Freer, R. (1998) An ion microprobe study of cation diffusion in diopside with applications to thermobarometry. Abstract, Mineralogical Society (London) Winter Meeting: *Microbeam Techniques in the Geosciences*, London, Jan. 1998.
- Béjina, F. and Jaoul, O. (1996) Silicon self-diffusion in quartz and diopside measured by nuclear microanalysis methods. *Phys. Earth Planet. Int.*, **97**, 145–62.
- Cawley, J.D. (1984) *Oxygen diffusion in alpha alumina*. Unpubl. PhD, Case Western Reserve University, 73 pp.
- Connolly, C. and Muehlenbachs, K. (1988) Contrasting oxygen diffusion in nepheline, diopside and other silicates and their relevance to isotopic systematics in meteorites. *Geochim. Cosmochim. Acta*, **52**, 1585–91.
- Dimanov, A. and Ingrin, J. (1995) Premelting and high-temperature diffusion of Ca in synthetic diopside: an increase of the cation mobility. *Phys. Chem. Min.*, **22**, 437–42.
- Dimanov, A., Jaoul, O. and Sautter, V. (1996) Calcium self-diffusion in natural diopside single crystals. *Geochim. Cosmochim. Acta*, **60**, 21, 4095–106.
- Elphick, S.C. and Graham, C.M. (1988) The effect of hydrogen on oxygen diffusion in quartz: Evidence for fast proton transients? *Nature*, **335**, 243–5.
- Elphick, S.C. and Graham, C.M. (1990) Hydrothermal oxygen diffusion in diopside at 1 kb, 900–1200°C, a comparison with oxygen diffusion in forsterite, and constraints on oxygen isotope disequilibrium in peridotite nodules. *Terra Abstr.*, **7**, 72.
- Farver, J.R. (1989) Oxygen self-diffusion in diopside with application to cooling rate determinations. *Earth Planet. Sci. Lett.*, **92**, 386–96.
- Farver, J.R. and Yund, R.A. (1990) The effect of hydrogen, oxygen and water fugacity on oxygen diffusion in alkali feldspar. *Geochim. Cosmochim. Acta*, **54**, 2953–64.
- Farver, J.R. and Yund, R.A. (1991) Oxygen diffusion in quartz: dependence on temperature and water fugacity. *Chem. Geol.*, **90**, 55–70.
- Fiquet, G., Gillet, P. and Richet, P. (1992) Anharmonicity and high-temperature heat capacity of crystals: the examples of CaGeO_4 , Mg_2GeO_4 and CaMgGeO_4 olivines. *Phys. Chem. Min.*, **18**, 469–79.
- Gérard, O. and Jaoul, O. (1989) Oxygen diffusion in San Carlos olivine. *J. Geophys. Res.*, **94**, 4119–28.
- Giletti, B.J. (1985) The nature of oxygen transport within minerals in the presence of hydrothermal water and the role of diffusion. *Chem. Geol.*, **53**, 197–206.
- Giletti, B.J. and Yund, R.A. (1984) Oxygen diffusion in quartz. *J. Geophys. Res.*, **89**, 4039–46.
- Huebner, J.S. and Voigt, D.E. (1988) Electrical conductivity of diopside: Evidence for oxygen vacancies. *Amer. Mineral.*, **73**, 1235–54.
- Ingrin, J., Latrous, K., Doukhan, J.C. and Doukhan, N. (1989) Water in diopside: an electron microscopy and infrared spectroscopy study. *Eur. J. Mineral.*, **1**, 327–41.
- Jaoul, O. and Raterron, P. (1994) High-temperature deformation of diopside crystal 3. Influences of $p\text{O}_2$ and SiO_2 precipitation. *J. Geophys. Res.*, **99**, 9423–39.
- Jaoul, O., Froidevaux, C., Durham, W.B. and Michaut, M. (1980) Oxygen self-diffusion in forsterite: implications for the high-temperature creep mechanism. *Earth Planet. Sci. Lett.*, **47**, 391–7.
- Jaoul, O., Houlier, B. and Abel, F. (1983) Study of ^{18}O diffusion in magnesium orthosilicate by nuclear microanalysis. *J. Geophys. Res.*, **88**, 613–24.
- Jaoul, O., Sautter, V. and Abel, F. (1991) Nuclear microanalysis: a powerful tool for measuring low atomic diffusivity with mineralogical applications. In *Diffusion, Atomic Ordering, and Mass Transport: Selected Topics in Geochemistry* (J. Ganguly, ed.). *Advances in Physical Geochemistry*, **8**, pp. 198–220. Springer-Verlag, Berlin, Heidelberg, New York.
- L'Hoir, A., Schmaus, D., Cawley, J. and Jaoul, O. (1981) Depth profiling light nuclei in single crystals: a combined nuclear reaction and RBS technique to minimize unwanted channeling effects. *Nucl. Inst. Methods*, **191**, 357–66.
- Reddy, K.P.R., Oh, S.M., Major, Jr., L.D. and Cooper, A.R. (1980) Oxygen diffusion in forsterite. *J. Geophys. Res.*, **85**, 322–6.
- Richet, P. and Fiquet, G. (1991) High-temperature heat capacity and premelting of minerals in the system $\text{MgO}-\text{CaO}-\text{Al}_2\text{O}_3-\text{SiO}_2$. *J. Geophys. Res.*, **96**, 445–56.
- Richet, P., Ingrin, J., Mysen, B.O., Courtial, P. and Gillet, P. (1994) Premelting effects in minerals: an experimental study. *Earth Planet. Sci. Lett.*, **121**, 589–600.
- Richet, P., Mysen, B.O. and Ingrin, J. (1998) High-Temperature X-ray diffraction and Raman spectroscopy of diopside and pseudowollastonite. *Phys. Chem. Min.*, **25**, 401–14.
- Ryerson, F.J. and McKeegan, K.D. (1994) Determination of oxygen self-diffusion in akermanite, anorthite, diopside, and spinel: Implication for oxygen isotopic anomalies and the thermal histories of Ca-Al-rich inclusions. *Geochim. Cosmochim. Acta*, **58**, 3713–34.
- Sneeringer, M., Hart, S.R. and Shimizu, N. (1984) Strontium and samarium diffusion in diopside. *Geochim. Cosmochim. Acta*, **48**, 1589–608.

- Stocker, R.L. (1978) Influence of oxygen pressure on defect concentrations in olivine with a fixed cationic ratio. *Phys. Earth Planet. Inter.*, **17**, 118–29.
- Stocker, R.L. and Smyth, D.M. (1978) Effect of enstatite activity and oxygen partial pressure on the point-defect chemistry of olivine. *Phys. Earth Planet. Int.*, **16**, 145–56.
- Weast, R.C. and Astle, M.J. (1979) *Handbook of Chemistry and Physics*. CRC Press Inc., Boca Raton, Florida.
- York, D. (1966) Least-squares fitting of a straight line. *Canad. J. Phys.*, **44**, 1079–86.
- Ziegler J.F. and Biersack, J.P. (1985) *The Stopping and Range of Ions in Solids*. Pergamon Press, New York.

[Manuscript received 2 October 1998;
revised 15 February 1999]